JOURNAL OF MATERIALS SCIENCE **40** (2005) 881 – 887

Electron transport behaviors across single grain boundaries in *n*-type $BaTiO_3$, $SrTiO_3$ and ZnO

TAKAHISA YAMAMOTO, YUKIO SATO, TOMOHITO TANAKA
Department of Advanced Materials Science, The University of Tokyo, 7-3-1 Hongo Bunkyo-ku Tokyo 113-8656, Japan
E-mail: yamataka@k.u-tokyo.ac.jp

KATSURO HAYASHI
ERATO, Japan Science and Technology Agency, KSP C-1232, Kawasaki 213-0012, Japan

YUICHI IKUHARA
Institute of Engineering Innovation, The University of Tokyo, 2-11-16 Yayoi Bunkyo-ku Tokyo 113-8656, Japan

TAKETO SAKUMA
Department of Advanced Materials Science, The University of Tokyo, 7-3-1 Hongo Bunkyo-ku Tokyo 113-8656, Japan

In some electroceramic materials, their unique electrical properties are due to potential barriers, i.e., double Schottky barriers (DSBs), formed at grain boundaries. So far, some researchers have revealed that the electrical properties of DSB are closely related to grain boundary characters, especially grain boundary coherency. For example, highly coherent boundary does not give PTCR or varistic property, while random types exhibit clear resistivity jump or abrupt current increment. Therefore, a concept of grain boundary design will be required for future device manufacturing, even in bulk materials. But it has not been clarified yet why the electron transport behaviors depend on them. In order to address this question, it is necessary to carry out a systematic experiment focusing on single grain boundaries using well-defined bicrystals.

In the present study, we have summarized our studies with a special interest in electron transport behavior across single grain boundaries for *n*-type $BaTiO_3$, $SrTiO_3$ and ZnO.
© *2005 Springer Science + Business Media, Inc.*

1. Introduction

Some electroceramic materials such as PTCR-thermistors, varistors, and so on often use unique electrical properties of potential barriers, i.e., double Schottky barriers (DSBs) formed at grain boundaries [1–3]. For example, PTCR (positive temperature coefficient of resistivity) effect observed in donor-doped $BaTiO_3$ polycrystals results from the temperature dependence of DSB, which is due to a change in dielectric constant in $BaTiO_3$ [4]. The dielectric constant shows a sharp peak at the ferro-para electric transition associated with a cubic-to-tetragonal phase transition at about 130°C. This rapid change gives a rapid increase of resistivity. On the other hand, varistors, which are widely used for surge devices, circuit protectors and so on, use the collapse of DSB over a critical voltage range [5]. The disappearance of DSB reduces the apparent resistivity. This reduction of resistivity gives a bypass of overloaded voltage to protect electric circuits.

These phenomena themselves are widely known in the field of electroceramic materials, however, the precise mechanism of electron transport behavior across DSB has not been clarified yet. This may be due to the fact that most studies performed in this field have been carried out using polycrystalline materials. From the viewpoint of grain boundary phenomena, we must give attention to the phenomena at single grain boundaries. So far, direct measurements of electrical properties across single grain boundaries have been performed by some researchers [6–10]. They have revealed that the electrical properties vary at each grain boundary, which means that DSBs are closely related to the grain boundary characters. In general, *n*-type DSBs are generated when electrons are trapped at interface states formed at grain boundaries. Therefore, it must be necessary to discuss the relationship between grain boundary characters and the electrical properties of interface states, in order to reveal the grain boundary character dependency of DSBs.

In this report, we summarize our studies focusing on the electrical properties across single grain boundaries in *n*-type $BaTiO_3$, $SrTiO_3$ and ZnO.

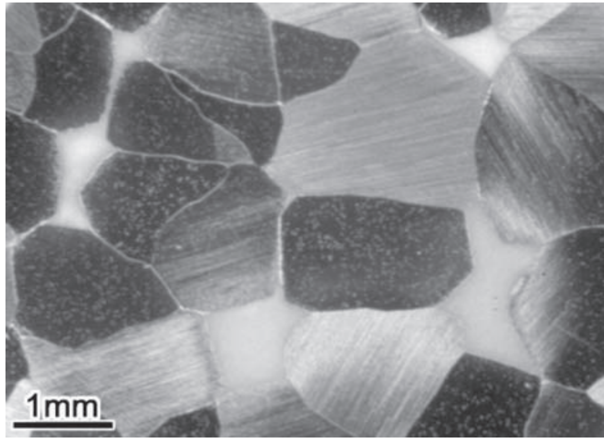

Figure 1 An optical micrograph in coarse-grained $BaTiO_3$ sinter. (Note that the grain size is about 1 mm.)

2. Grain orientation dependence of PTCR effect in Nb-doped $BaTiO_3$

In order to carry out direct measurements at single grain boundaries, it is suitable to use bicrystals with ideal grain boundaries, which are prepared by joining two specially oriented single crystals. For this purpose, it is technically important to prepare single crystals with a moderate size. But, in the case of $BaTiO_3$, it is not so easy to prepare single crystals suitable for bicrystal fabrication [11, 12] because $BaTiO_3$ has a hexagonal-cubic transformation at about 1430°C [13]. So, firstly, we prepared coarse-grained sinters large enough to apply micro electrodes on grain interiors as shown in Fig. 1. Using the sinters, systematic investigation across single grain boundaries will be possible without bicrystals [14]. It is noted that the grain size reaches about 1 mm in spite of the ordinary sintering condition. Such unique structures can be easily obtained by carefully choosing the type and amount of dopants. In order to grow grains as large as possible, it is necessary to keep the A/B ratio constant to be 0.9995 by doping, where the A/B ratio means a cation ratio in a perovskite structure of ABO_3 [14, 15].

Fig. 2a shows the temperature dependence of the resistance obtained from various types of single grain boundaries. The curves vary at each grain boundary. But the behavior can be roughly classified into two groups from the viewpoint of a magnitude of resistance jump, i.e., the boundaries exhibiting clear jump and no or small jump. These features are depending on the coherency of grain boundaries. The coherency of the grain boundary is often discussed in terms of coincidence site lattice (CSL) theory, which describes the degree of lattice site matching between two adjacent grains. According to CSL theory [16], the boundaries are roughly classified into coherent boundaries called as Σ boundaries, and into random type boundaries. As shown in Fig. 2a, the high coherent boundaries such as low angle, $\Sigma 3$ and $\Sigma 9$ boundaries show no resistance jump, while the other random boundaries exhibit clear resistance jump. The relation between PTCR effect and boundary coherency can be also confirmed by misfit dependency of a magnitude of the resistance jump. Fig. 2b shows the resistance curves taken from $\Sigma 3$ boundaries without and with some misfit angles. As shown in Fig. 2b, the magnitude of resistance jump increases with a misfit angle from an exact $\Sigma 3$ relation. The boundary having a misfit angle of $\sim 9^\circ$ exhibits a clear resistance jump as in the curve 6.

When a boundary has a misfit angle from a perfect Σ relation, DSC (displacement shift compete) dislocations are introduced into the boundary to accommodate the misfit angle. Considering the overlap of DSC dislocation cores, the allowance of the angle can be written as follows,

$$0 \leq \Delta\theta \leq \frac{15}{\sqrt{\Sigma}}$$

where $\Delta\theta$ is an allowing misfit angle. In the case of $\Sigma 3$ boundary, a limit of $\Delta\theta$ is estimated to be 8.7°.

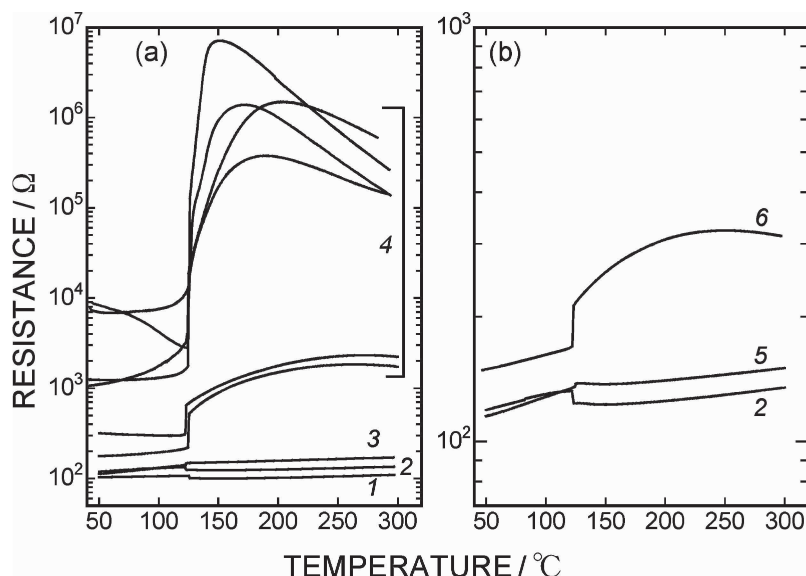

Figure 2 (a) Resistance-temperature characteristics taken from various types of single grain boundaries in n-type $BaTiO_3$ sinters as shown in Fig. 1, a low angle boundary in the curve 1, $\Sigma 3$ in the curve 2, $\Sigma 9$ in the curve 3 and random type in the curve 4. (b) Misfit angle dependence of $\Sigma 3$ boundary without misfit in the curve 2, with a misfit angle of 4° in the curve 5 and of 9° in the curve 6.

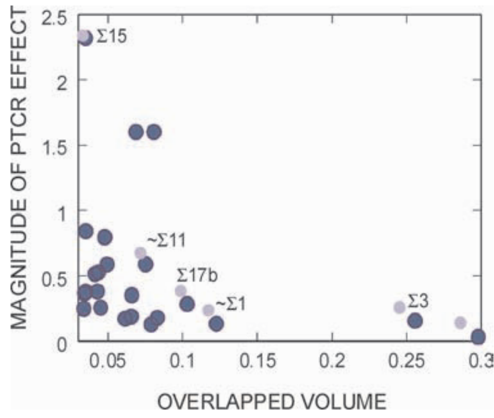

Figure 3 A plot of a magnitude of PTCR effect as a function of overlapped volume of V_{gG}.

As shown in the curve 6, the boundary having a misfit angle of $\sim 9^{\circ}$ exhibits a clear jump even though PTCR effect does not appear in the boundary having the lower misfit angles as in the curves 2 and 5.

On the other hand, PTCR effect also varies even in a group of random type boundaries as in the Fig. 2a. In general, CSL theory cannot distinguish between different degrees of randomness at random type boundaries. For that case, there is a convenient method proposed by Ikuhara and Pirouz, which is called CRLP (coincidence of reciprocal lattice points) method [17]. This concept was originally used to find an energetically-favorable orientation relationship at interphase boundaries, and can be applied to evaluate the coherency of grain boundaries having a various type of boundaries [18]. In this concept, coherency is determined using an overlap volume V_{gG} of reciprocal lattice points obtained from respective lattices of two adjacent grains when some volume is given to each reciprocal point. For instance, V_{gG} is unity for an exact $\Sigma 1$ boundary and takes a high value for $\Sigma 3$ or $\Sigma 9$ boundary while random boundaries are characterized by lower values of V_{gG}. Fig. 3 is a plot of the magnitude of PTCR effect against the overlapped volume of V_{gG} [19]. The magnitude is a ratio of the maximum to minimum resistance for each boundary in a temperature range of 50 to 300°C. The PTCR effect can be described as a function of overlapped volume. This result indicates that the magnitude of PTCR effect can be controlled if one can control the coherency of a single grain boundary.

As mentioned above, the electrical properties across grain boundaries depend on the coherency of the grain boundaries. But, a question arises, namely, why does electrical property change with a variation of coherency of grain boundaries? In order to clarify this point, we carried out bicrystal experiments using Nb-doped $SrTiO_3$, which are similar type electroceramic materials to n-type $BaTiO_3$.

3. Effects of point defects on the electron transport behavior in Nb-doped $SrTiO_3$ bicrystals

DSB in n-type semiconductors is generated by electronic charges trapped at interface states at grain boundaries, and therefore, the electron transport behavior is closely related to energetic features in the band gap due to interface states. For example, atomic disorder at grain boundaries are known to be associated with active interface states in the case of doped Si [20, 21]. This is because dangling bonds or rearrangements of atoms at grain boundaries often form extra electronic states in the band gap, which behave as acceptor like states. On the other hand, in the case of electroceramic materials, point defects that are negatively charged play an important role to the formation of interface states [22].

Fig. 4a shows a HRTEM image in a low angle boundary of 0.1at%Nb-doped $SrTiO_3$ bicrystals joined at 1400°C for 10 h in air [23]. In the figure, the electron beam direction is nearly parallel to [001] of both crystals, and the boundary is set at an edge-on condition. The boundary can be confirmed to be joined at an atomic scale, and the boundary is free from any secondary phases. The inset figure is a selected area

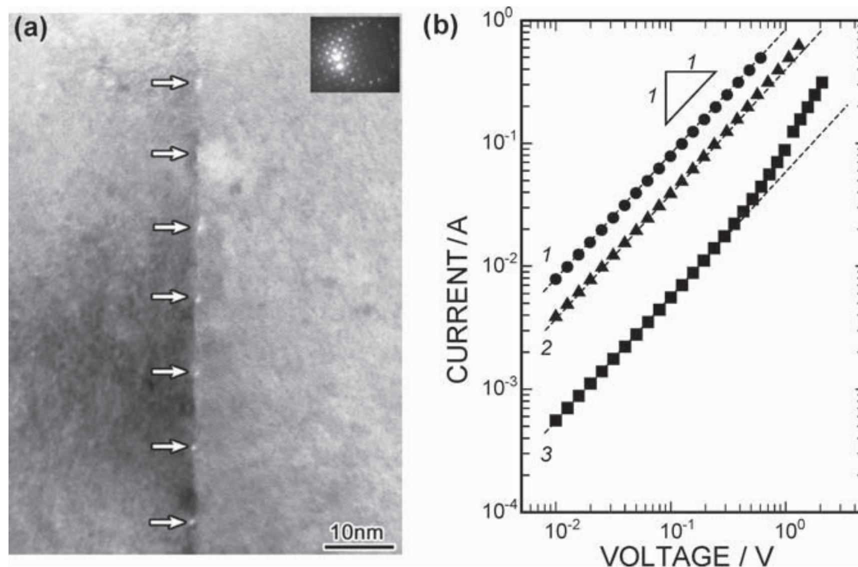

Figure 4 (a) HRTEM image taken from a low angle boundary with a rotation angle of 1.7°, (b) current-voltage relations from $\Sigma 1$ in the curve 1 and low angle boundaries cooled with a cooling rate of 200°C/h in the curve 2 and 50°C/h in the curve 3. In the figure (a), the arrows indicate grain boundary dislocations.

diffraction pattern taken from the both crystals. From the Kikuchi lines appearing in the pattern, a misfit angle between the adjacent crystals is estimated to be about 1.7°, including both a tilt and a twist type components. There can be seen particular contrasts along the boundary as indicated by the arrows. These contrasts are due to grain boundary dislocations, which are introduced in order to accommodate the misfit angle between the two adjacent crystals.

Fig. 4b shows a plot of current-voltage behavior obtained from low angle boundaries, which were prepared with different cooling rates after joining. In the figure, the data obtained from $\Sigma 1$ boundary without any misfits is also shown for comparison. The $\Sigma 1$ boundary exhibits linear current-voltage relation, i.e., Ohmic relation, as often observed in single crystals, indicating no experimental errors such as incorporating some impurities and so on. On the other hand, both low angle boundaries exhibit slight non-linearity, which arises from DSB formed at the grain boundary. However, the non-linearity changes by a variation of cooling rates after joining. Reduction of a cooling rate gives larger non-linearity (Fig. 4b, the curve 3). The important point to note is that these two boundaries consist of grain boundary dislocations as seen in Fig. 4a. The number and the spacing of the grain boundary dislocations in a low angle boundary depend on the misfit angle, so that the grain boundary structure cannot be considered to change unless the misfit angle changes. Namely, the grain boundary structure is the same between the two boundaries as in the figure (b) even if the cooling rates are different. This fact suggests that the change of electrical properties obtained in the current-voltage curves is closely related to point defect chemistry, not directly to the change in atomic structure.

This phenomenon can be explained by considering an accumulation of cation type vacancies, i.e., negatively charged point defects.

$SrTiO_3$ lattice structure has Schottky type defects as follows,

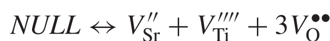

$$NULL \leftrightarrow V''_{Sr} + V''''_{Ti} + 3V^{\bullet\bullet}_{O}$$

These defects are considered to be generated or annihilated at distorted areas such as dislocations, surfaces, grain boundaries and so on, because a reaction of this type requires the generation or annihilation of excess vacant sites. During annealing, a flow of point defects takes place from source area, i.e., grain boundary dislocations, to grain interior. At this time, the generation rate of point defects is governed by a difference in the formation energy of point defects [24, 25]. In the case of $SrTiO_3$, the formation energy of cation vacancies is considered to be lower comparing with that of anion vacancies. As a result, cation type defects tend to segregate around grain boundary dislocation. This process is an equilibrium process due to energetic difference of point defect formation. On the other hand, the effect of non-equilibrium process becomes significant on cooling. When samples are cooled with a certain cooling rate, a flow from grain interior to a grain boundary dislocation takes place to reduce their concentration at lower temperature. At this time, point defects that have higher diffusivity tend to recover faster than the others. In the case of $SrTiO_3$, the diffusivity of oxygen ions is considered to be the fastest. As a result, cation type defects are accumulated around grain boundary dislocations. When these acceptor type defects such as negatively-charged V''_{Sr}, V''''_{Ti} and so on accumulate at grain boundaries, a charge imbalance takes place, and then, potential barriers of DSB are formed [22, 26, 27].

Fig. 5 shows a schematic of the accumulated area formed around grain boundary dislocations. The area spreads to have a certain radius centering at respective grain boundary dislocations. The radius is depending on a cooling rate within a certain cooling rate. These areas trap the electrons that form DSBs.

In random type boundaries, the accumulating effects become significant because of their low coherency. Fig. 6a and b show a HRTEM image in the vicinity of random type boundary, whose tilt angle is 45° as seen in the inset diffraction pattern, and the current-voltage behavior obtained from the boundary [28]. No secondary phase can be observed in the vicinity of the grain boundary despite a part of the boundaries being faceted with {210} type planes [29]. The boundary exhibits clear non-linearity as in Fig. 6b, but the current-voltage relation has a distinct feature. In general, simple DSB exhibits three kinds of current-voltage

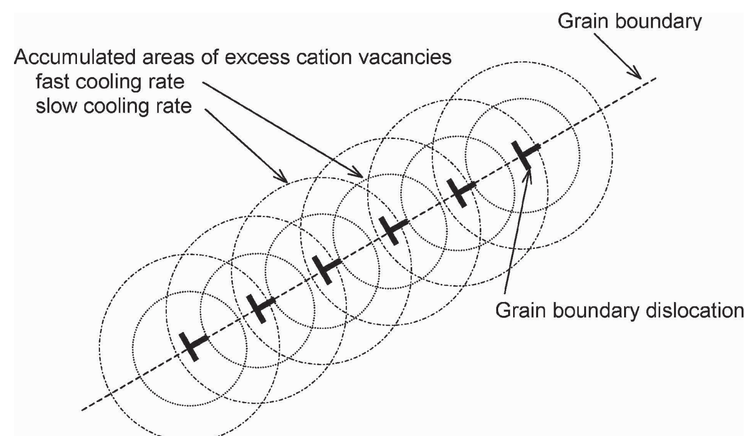

Figure 5 A schematic showing accumulated areas of cation type point defects formed around grain boundary dislocations.

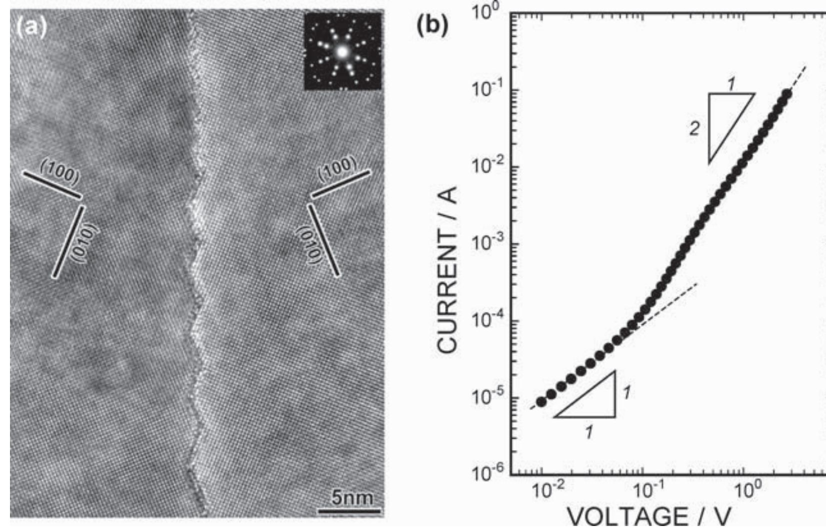

Figure 6 (a) HRTEM image in the vicinity of [001] symmetrical tilt boundary with a tilt angle of 45°, (b) current-voltage behavior taken from the boundary.

dependencies, i.e., Ohmic($\alpha = 1$), sub-Ohmic($\alpha < 1$) and exponential regions with an increase in the applied voltage, where α, a coefficient of non-linearity, is defined as $\partial \log I / \partial \log V$ [30]. Comparing with the simple DSB, the current-voltage relation seen in Fig. 6b has two characteristic features, i.e., absence of sub-Ohmic dependency and appearance of quadratic dependency as indicated in the figure. Both features may be considered to be due to electron transport through a wide insulating intermediate layer [31]. But, it is noted that the boundary has no secondary phases as seen in HRTEM image of Fig. 6a. Namely, an insulating layer to give $\alpha = 2$ relation in current-voltage behavior is due to the accumulation of acceptor type point defects widely distributed at grain boundary. Such areas cannot be directly observed by HRTEM because point defects do not give a different structure comparing with a $SrTiO_3$ structure.

So far, several examinations at single grain boundaries have been carried out, and it was confirmed that the electron transport behavior depends on grain orientation relationship. The reason for such phenomena can be considered that the accumulating behavior of acceptor type point defects depends on grain orientation relation.

4. The number of electrons necessary to form DSB by one grain boundary dislocation

As mentioned above, the accumulation of acceptor type point defects gives the electronic charge necessary to form DSB. In the case of low angle boundaries, the source of them is considered to be grain boundary dislocations. Then, we can estimate the number of electrons related to one grain boundary dislocation by using low angle boundaries having different misfit angles.

Fig. 7 shows HRTEM images taken from two kinds of low angle symmetric [001] tilt boundaries. The boundaries were prepared to have tilt angles of 2° and 4°, respectively. The boundary consists of grain boundary dislocations similar to that as shown in

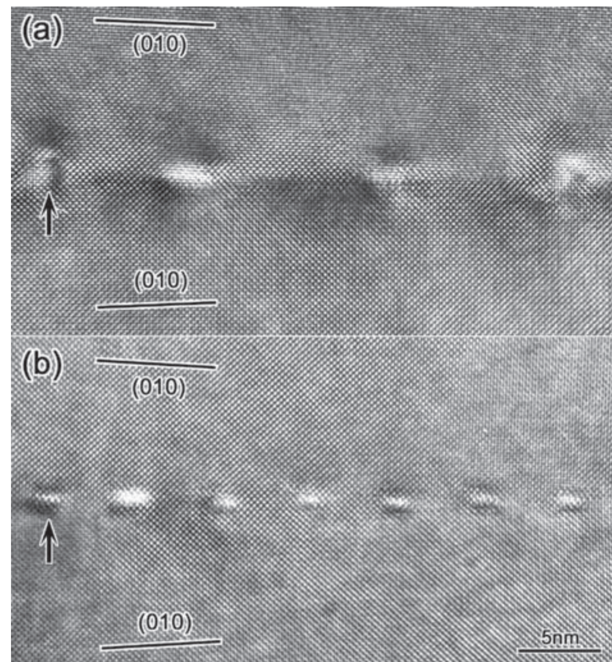

Figure 7 HRTEM images of low angle tilt boundaries with a tilt angle of (a) 2° and (b) 4°.

Fig. 4a. But, the number of them is different because the tilt angle changes. The average spacing of grain boundary dislocations in each boundary are 10 nm in the 2°-boundary and 5.7 nm in the 4°-one, respectively. Fig. 8 shows current-voltage characteristics across the boundaries as shown in Fig. 7. The current-voltage behavior clearly deviates from linear to non-linear relationship over the voltage in both boundaries. However, the non-linearity, α, increases with an increase in a misfit angle, i.e., about 1.2 in the 2°-boundary and about 1.7 in the 4°-one, respectively. Considering the HRTEM results as in Fig. 7, it is obvious that electrical properties across low angle boundaries are closely related to the number of grain boundary dislocations.

The number of trapped electrons can be roughly estimated using a simple DSB model from the maximum

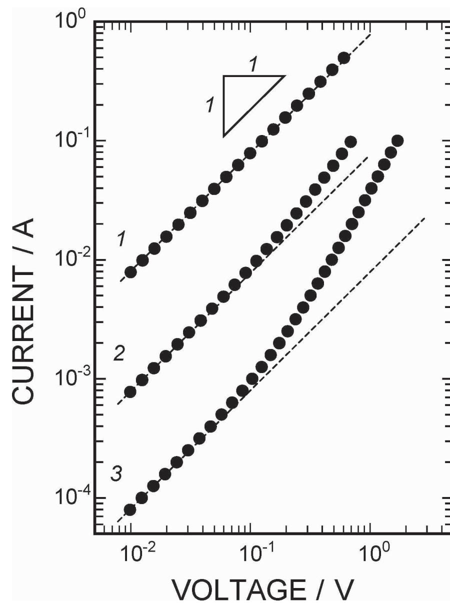

Figure 8 Current-voltage relations taken from Σ1 boundary in the curve 1 and low angle boundaries with a tilt angle of 2° in the curve 2 and 4° in the curve 3.

value, α_{max}, of the non-linearity coefficient using the following equation [32],

$$\alpha_{max} = \frac{S^2\phi_0}{2kT} = \frac{S^2Q^2}{16\varepsilon_0\varepsilon_r kTN_d},$$

where ϕ_0 is the height of DSB without bias voltage, N_d carrier density, S the ratio of Q_V and Q, respectively. Q and Q_V are grain boundary charge densities without and with bias voltage. Here, the value of S is assumed to be 1, and we assume a relative dielectric constant of ε_r as 500. Using the respective α value for each current-voltage relation, the number of electrons contributing to form DSB is estimated to be 2.0×10^{13} cm^{-1} in the 2°-boundary and 2.4×10^{13}cm^{-1} in the 4°-boundary. Recently, Zhang *et al*. have revealed core structures of the dislocations in undoped $SrTiO_3$ bicrystal having a [001] symmetric tilt boundary with a tilt angle of 5.4° [33]. According to their results, the dislocation core exhibits slight dissociation on the {100} plane. The dislocation examined in the present study possibly has a similar structure to that they observed. As for the calculations described here, the dislocation structure as shown in Fig. 7 was treated as a simple edge type dislocation.

Fig. 9 shows a plot of the number of electrons as a function of dislocation density estimated from both low angle boundaries. In the figure, the number of electrons increases with misfit angle. By calculating a ratio of the increment of each value, i.e., the number of electrons and dislocation density, we can estimate the number of electrons contributed by one grain boundary dislocation having a unit length. The value is 5.0×10^6 cm^{-1}. Namely, the length of a dislocation necessary to contribute to put out one electron is about 2 nm. This value is noted to be related to the imbalanced amount between negatively and positively charged-up point defects, which are distributed around grain boundary dislocations. It is not directly related to the defect content itself.

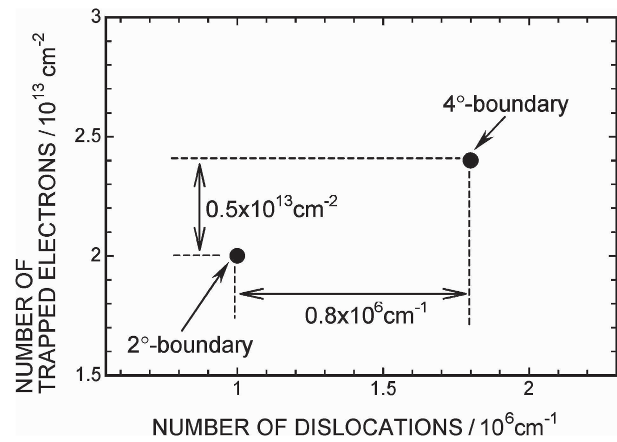

Figure 9 A plot of the estimated number of electrons necessary to form DSB as a function of a density of grain boundary dislocations.

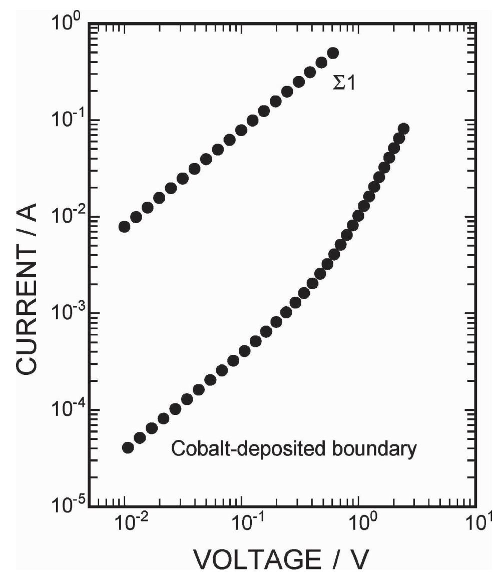

Figure 10 Current-voltage behavior in cobalt-deposited Σ1 boundary.

5. DSB at a chemical boundary

We can create DSB only by segregating a specific ion whose electronic structure is suitable for serving acceptor states irrespective of a lattice structure. The preparation of this unique bicrystals was made by a way that metallic Co was evaporated on a (100) surface of a single crystal and then joined with another single crystal with a clean (100) surface to have the same orientation relationship. A linear current-voltage characteristic as in Fig. 9 is obtained in the clean Σ1 boundary, while the current is very much reduced and nonlinear relation clearly appears in the Co-deposited Σ1 boundary [34]. This result indicates that the presence of some sort of ions can give DSB in grain boundaries irrespective of atomic structural effect.

6. Grain orientation dependence of DSB in ZnO bicrystals

In the case of the materials as mentioned above, electron transport behavior across grain boundaries varies with grain boundary characters. But, all of electroceramic materials do not always exhibit such grain orientation dependency of electrical properties. Fig. 11 shows

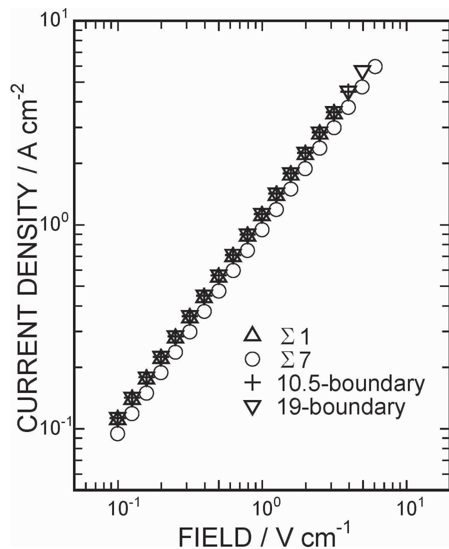

Figure 11 Current-voltage characteristics in various types of twist boundaries of undoped ZnO bicrystals.

current-voltage behavior in various types of boundaries in undoped ZnO bicrystals [35]. As seen in the figure, clear Ohmic relations can be observed in all types of the boundaries.

The difference between the former materials and ZnO are mainly originated from the difference in intrinsic type of defects. $BaTiO_3$ and $SrTiO_3$ have Schottky type of defect reaction while ZnO has cation excess Frenkel type. In the case of interstitial cation defects, if the defects will be introduced and accumulated at grain boundaries, they can not directly operate as acceptor type defects. In order to form DSB at grain boundaries, additional dopants such as Co, Pr and so on, must be necessary, which serve acceptor states in a band gap [36].

7. Conclusions

We reviewed our research for electron transport behaviors across single grain boundaries performed for n-type $BaTiO_3$, $SrTiO_3$ and ZnO. The electrical properties across single grain boundaries in n-type $BaTiO_3$ and $SrTiO_3$ depend on the grain boundary coherency. Double Schottky barriers (DSBs) are not formed or their height becomes small at highly coherent boundaries, while they are clearly generated at low coherent boundaries. Bicrystal experiments performed for Nb-doped $SrTiO_3$ have revealed that the formation of DSBs is due to the accumulating behaviors of acceptor type defects around grain boundaries. The variation of electrical properties across single grain boundaries can be concluded to result in such accumulating behaviors of acceptor type defects which are depending on the grain boundary characters. On the other hand, the electrical properties in undoped ZnO did not exhibit grain boundary dependency. This is because electronic features in the band gap do not give active acceptor states if some dangling bonds or atomic rearrangement are formed at grain boundaries.

In this field, it is very important to understand defect chemistry from a viewpoint of their electronic states, e.g., localized quantum structures caused by point defects. To understand them gives a new concept for developing unique properties in a field of electroceramic materials.

References

1. B. HUYBRECHTS, K. ISHIZAKI and M. TANAKA, *J. Mater. Sci.* **30** (1995) 2463.
2. TAPAN K. GUPTA, *J. Am. Ceram. Soc.* **73** (1990) 1817.
3. L. HOZER (eds.), "Semiconductor Ceramics" (Ellis Horwood, Poland, 1994).
4. W. HEYWANG, *J. Mater. Sci.* **6** (1971) 1214.
5. G. D. MAHAN, L. M. LEVINSON and H. R. PHILIPP, *J. Appl. Phys.* **50** (1979) 2799.
6. P. GERTHSEN and B. HOFFMANN, *Solid State Electron.* **16** (1973) 617.
7. H. NEMOTO and I. ODA, *J. Am. Ceram. Soc.* **63** (1980) 398.
8. M. KUWABARA, K. MORIMO and T. MATSUNAGA, *ibid.* **79** (1996) 997.
9. M. NOMURA, N. ICHINOSE, H. HANEDA and J. TANAKA, *Key Eng. Mater.* **157-158** (1999) 207.
10. S. RODEWALD, J. FLEIG and J. MAIER, *J. Euro. Ceram. Soc.* **19** (1999) 797.
11. J. P. REMEIKA, *J. Am. Chem. Soc.* **76** (1954) 940.
12. D. RYTZ, B. A. WECHSLER, C. C. NELSON and K. W. KIRBY, *J. Cryst. Growth* **99** (1990) 864.
13. K. W. KIRBY and B. A. WECHSLER, *J. Am. Ceram. Soc.* **74** (1991) 1841.
14. K. HAYASHI, T. YAMAMOTO and T. SAKUMA, *ibid.* **79** (1996) 1669.
15. T. YAMAMOTO, *British Ceram. Trans.* **94** (1995) 196.
16. D. G. BRANDON, B. RALPH, S. RANGANATHAN and M. S. WALD, *Acta Metal.* **12** (1964) 813.
17. Y. IKUHARA and P. PIROUZ, *Mater. Sci. Forum* **207–209** (1996) 121.
18. Y. IKUHARA and P. PIROUZ, *Micros. Res. Tech.* **40** (1998) 206.
19. K. HAYASHI, T. YAMAMOTO, Y. IKUHARA and T. SAKUMA, *J. Am. Ceram. Soc.* **83** (2000) 2684.
20. C. H. SEAGER and G. E. PIKE, *Appl. Phys. Lett.* **35** (1979) 709.
21. M. KOHYAMA and R. YAMAMOTO, *Phys. Rev. B.* **49** (1994) 17102.
22. J. DANIELS and R. WERNICKE, *Philips Res. Repts.* **31** (1976) 544.
23. T. YAMAMOTO and Y. IKUHARA, *J. Elec. Micros.* **50** (2001) 485.
24. Y.-M. CHIANG and T. TAKAGI, *J. Am. Ceram. Soc.* **73** (1990) 3278.
25. S. B. DESU and D. A. PAYNE, *J. Am. Ceram. Soc.* **73** (1990) 3391.
26. J. NOWOTNY, *Ceram. Inter.* **17** (1991) 227.
27. Y.-M. CHIANG and T. TAKAGI, *J. Am. Ceram. Soc.* **73** (1990) 3286.
28. T. YAMAMOTO, Y. IKUHARA and T. SAKUMA, *J. Mater. Sci. Lett.* **20** (2001) 1827.
29. T. YAMAMOTO, K. HAYASHI, Y. IKUHARA and T. SAKUMA, *J. Mater. Res.* **13** (1998) 3449.
30. G. E. PIKE and C. H. SEAGER, *J. Appl. Phys.* **50** (1979) 3414.
31. K. HAYASHI, T. YAMAMOTO, Y. IKUHARA and T. SAKUMA, *ibid.* **86** (1999) 1.
32. K. MUKAE, *Key Eng. Mater.* **125–126** (1997) 317.
33. Z. ZHANG, W. SIGEL and M. RUHLE, *Phys. Rev.* **B66** (2002) 094108.
34. T. YAMAMOTO, K. HAYASHI, Y. IKUHARA and T. SAKUMA, *J. Am. Ceram. Soc.* **83** (2000) 1527.
35. Y. SATO, F. OBA, T. YAMAMOTO, Y. IKUHARA and T. SAKUMA, *ibid.* **85** (2002) 2142.
36. Y. SATO, T. MIZOGUCHI, F. OBA, M. YODOGAWA, T. YAMAMOTO and Y. IKUHARA, *Appl. Phys. Lett.* **84** (2004) 5311.